GEOPHYSICS, VOL. 60, NO. 6 (NOVEMBER-DECEMBER 1995); P. 1897-1905, 12 FIGS.

An elastodynamic inverse scattering method for removing scattered surface waves from field data

Bastian Blonk*, Gerard C. Herman‡, and Guy G. Drijkoningen**

ABSTRACT

In an earlier paper, we introduced a 3-D inverse scattering method for removing scattered surface waves from seismic data that was based on a tomographic imaging of the scattered surface waves by a data-fitting procedure that used as much of the seismic data as possible. After this imaging step, the scattered surface waves can be computed and removed for each separate source-receiver pair. We now apply the method to two field-data sets. The method requires a knowledge of the source waveform and shallow propagation characteristics, and these input requirements are estimated from the direct surface wave. We conclude that the method effectively attenuates crossline scattered surface waves without affecting deeper reflections.

INTRODUCTION

In many cases, the shallow subsurface of the earth is strongly heterogeneous. This heterogeneity can significantly deteriorate the quality of land seismic data when it gives rise to strong near-surface scattering of seismic waves. In a number of cases, near-surface scattering consists mainly of scattered surface waves (ground roll). Inline scattered surface waves can be removed by using filtering techniques (see, for instance, Yilmaz, 1988, section 1.6.2). However, crossline scattered surface waves, which can be present to a considerable degree, are left partially intact by these widely used techniques because they can have a high apparent phase velocity, show hyperbolic moveout, and arrive later in the section at small offsets. Therefore, crossline scattered surface waves can resemble body-wave reflections from the deeper part of the subsurface.

In previous papers, we discussed a method for eliminating both inline and crossline scattered surface waves (Blonk and Herman, 1993; 1994). This procedure was based on elastodynamic inverse scattering theory and consisted of two steps. In the first step, we estimated a near-surface scattering model using as many seismic data as possible. In the second step, for each separate source-receiver pair, this scattering model was used to compute and eliminate the scattered surface waves.

Our previous papers showed that the method is effective for synthetic data. The technique is not sensitive to the parameterization of the scattering model (e.g., type of contrast, discretization cells); however, it is sensitive to the Rayleigh wave speed. This sensitivity is comparable to the sensitivity to body wave speed of methods like prestack depth migration and linearized inversion.

In this paper, we apply our method to two different field-data sets, and we show that the Rayleigh wave speed, as well as other characteristics of the surface wave, can be obtained directly from the data with sufficient accuracy. The first data set was recorded in February 1993 in a "controlled" experiment. In this experiment, the actual near-surface scatterer distribution was known. From this experiment, we conclude that our method is applicable to field data and also that it can take dispersion into account. The second data set is a seismic line strongly contaminated with scattered surface waves. This contamination is such that no coherent reflections can be distinguished in several parts of the stack. We have found that, after application of our method, an improvement of the stack is obtained.

DESCRIPTION OF THE METHOD

This section briefly summarizes the elastodynamic inverse scattering method discussed in our previous papers (Blonk and Herman, 1993; 1994). It also describes a new estimation procedure of the source signature and shallow propagation characteristics from the direct surface wave.

Manuscript received by the Editor February 24, 1994; revised manuscript received February 10, 1995.
*Formerly Dept. of Applied Mathematics, Delft University of Technology, Mekelweg 4, 2628 CD Delft, The Netherlands; Presently Shell Research Volmerlaan 6, 2288 GD Rijswijk, The Netherlands.
‡Dept. of Applied Mathematics, Delft University of Technology, Mekelweg 4, 2628 CD Delft, The Netherlands.
**Dept. of Mining and Petroleum Engineering, Delft University of Technology, Mijnbouwstraat 120, 2628 RX Delft, The Netherlands.

Formulation of the forward and inverse problems

We consider scattering of elastic waves by inhomogeneities embedded in a half-space V bounded by a stress-free surface ($x_3 = 0$). The wavefield is generated by a vertical stress source located at surface position x^s. In this paper, we consider only the vertical component of the total particle velocity field v_3, which is recorded at surface position x.

First, we formulate the forward problem. Starting from the frequency-domain forms of the linearized equation of motion and the linearized equation of deformation of an elastic solid, we can derive a domain-type integral representation for the wavefield with the aid of the Betti-Rayleigh reciprocity relation. The wavefield v3 can be written as a superposition of the incident field v_3^{inc} and the scattered field v_3^{sc}, i.e.,

$$v_3(\mathbf{x}, \mathbf{x}^s) = v_3^{inc}(\mathbf{x}, \mathbf{x}^s) + v_3^{sc}(\mathbf{x}, \mathbf{x}^s). \quad (1)$$

The incident wavefield v_3^{inc} is given by

$$v_3^{inc}(\mathbf{x}, \mathbf{x}^s) = W v_{33}^G(\mathbf{x}|\mathbf{x}^s), \quad (2)$$

where $W = W(\omega)$ is the amplitude spectrum of the stress source and ω denotes the angular frequency. The quantity $v_{ij}^G(\mathbf{x}|\mathbf{x}')$ denotes the Green's velocity tensor of a suitably chosen background medium, i.e., the x_i-component of the velocity field in this background medium at position x caused by an impulsive stress source directed along the positive xj-axis and located in x' [in equation (2), i = j = 3]. The dependence on ω of v_3, v_3^{inc}, v_3^{sc}, and v_{ij}^G is omitted for brevity throughout this paper. We assume that the deviation of the actual medium from the background medium is so small that the problem can be linearized and, therefore, we apply the Born approximation. For a contrast in mass density, the scattered wavefield v_3^{sc} is then given by

$$v_3^{sc}(\mathbf{x}, \mathbf{x}^s) = i\omega W \int_V dV(\mathbf{x}')(\rho(\mathbf{x}') - \rho^{(0)}(\mathbf{x}'))G_3^p(\mathbf{x}'|\mathbf{x}, \mathbf{x}^s), \quad (3)$$

where ρ and $\rho^{(0)}$ are the mass densities of the actual and the background medium, respectively, and i is the imaginary unit. The quantity G_3^p describes the propagation effects and is given by

$$G_3^p(\mathbf{x}'|\mathbf{x}, \mathbf{x}^s) = -(v_{31}^G(\mathbf{x}|\mathbf{x}')v_{13}^G(\mathbf{x}'|\mathbf{x}^s) + v_{32}^G(\mathbf{x}|\mathbf{x}')v_{23}^G(\mathbf{x}'|\mathbf{x}^s) + v_{33}^G(\mathbf{x}|\mathbf{x}')v_{33}^G(\mathbf{x}'|\mathbf{x}^s)). \quad (4)$$

For elasticity contrasts, expressions for the scattered wavefield are comparable to expressions (3) and (4) (Blonk and Herman, 1994).

Next, we formulate the inverse problem. Its objective is the elimination of scattered surface waves without affecting the deeper reflections. We are dealing here with surface waves that have been scattered by inhomogeneities near the surface. Since such inhomogeneities can be approximated effectively by a 2-D contrast function (Aki, 1969), we assume that the mass density contrasts are present in one shallow layer at depth level $\bar{x}_3$. The thickness of the layer is small compared to the seismic wavelength. We have shown that the sensitivity of the method to neglecting contrasts in elasticity is rather low (Blonk and Herman, 1994); therefore, these contrasts will not be considered here.

The wavefield $\bar{v}_3$ that specifically accounts for the near-surface effects is now given as

$$\bar{v}_3(\mathbf{x}, \mathbf{x}^s) = v_3^{inc}(\mathbf{x}, \mathbf{x}^s) + i\omega W \int_{IR^2} dA(\boldsymbol{\nu}')\xi(\boldsymbol{\nu}')G_3^{shallow}(\mathbf{x}'|\mathbf{x}, \mathbf{x}^s). \quad (5)$$

In equation (5), ξ is the distribution of scatterers (contrast function) in the layer (it equals the product of the layer thickness and a contrast in mass density), $\boldsymbol{\nu}'$ denotes the 2-D vector (x_1', x_2'), and $x' = (\boldsymbol{\nu}', \bar{x}_3)$. Note that ξ depends only on the horizontal coordinates x_1' and x_2'; the dependence on x_3' is neglected since the layer is thin. From tests on synthetic data, we have observed that for shallow scatterers, $G_3^{shallow}$ can be approximated by its surface-wave part:

$$G_3^{shallow}(\mathbf{x}'|\mathbf{x}, \mathbf{x}^s) \simeq -v_{33}^{G,s}(\mathbf{x}|\mathbf{x}')v_{33}^{G,s}(\mathbf{x}'|\mathbf{x}^s), \quad (6)$$

where $v_{33}^{G,s}$ denotes the surface-wave part of the Green's tensor v_{33}^G. This surface-wave part can be isolated from v_{33}^G with the aid of high-frequency asymptotics (Blonk and Herman, 1994). In the next subsection, we will describe how we can estimate $G_3^{shallow}$ from the direct surface wave. Having determined $G_3^{shallow}$, we estimate the contrast function ξ by minimizing a squared L^2 norm of the difference between the actual wavefield v_3 and the wavefield $\bar{v}_3$ that accounts for the near-surface effects [as given in equation (5)]. The L^2 norm is, in the time-domain, given by

$$\sum_{\substack{sources \\ receivers \\ times}} [h^{time}(v_3^{time} - \bar{v}_3^{time})]^2, \quad (7)$$

where v_3^{time} and $\bar{v}_3^{time}$ are time-domain counterparts of v_3 and $\bar{v}_3$, respectively. The function h^{time} [$= h^{time}(x, \mathbf{x}^s, t)$, where t denotes time] is a window function that suppresses the part of the wavefield that contains no near-surface scattered waves: the direct surface wave and the wavefield arriving prior to it. Minimizing equation (7) can be done in the frequency domain, and it can be shown that it is then equivalent to determining

$$\min_{\boldsymbol{\xi}} \|\mathbf{d} - \underset{\sim}{\mathbf{K}}\boldsymbol{\xi}\|, \quad (8)$$

where $\|\cdot\|$ denotes the L^2 norm. For all sources, receivers, and frequencies involved, the vector d contains terms $h * \bar{v}_3$, while the matrix $\underset{\sim}{\mathbf{K}}$ contains $h * \bar{v}_3$ in terms of $G_i^{shallow}$ and the amplitude spectrum W of the stress source ($*$ denotes convolution and h is the frequency-domain counterpart of h^{time}). The discretized contrast function ξ is represented by the vector $\boldsymbol{\xi}$. To solve the condition (8), we employ a conjugate gradient method [see, for instance, Kleinman and van den Berg (1991) for details].

We emphasize that the inversion as defined in statement (8) is actually a data-fitting procedure; any set of model parameters that minimizes the condition (8) is accepted. Consequently, it is important to realize that our aim is not to determine the actual (unique) near-surface scatterer distribution, but only some contrast function ξ that enables us to calculate, approximately, the surface-scattered part of v_3. This explains why a mass density contrast can also be used to eliminate surface waves scattered by elasticity contrasts.

After estimating ξ according to condition (8) from as many seismic data as possible, the scattered surface waves are computed for each experiment using relationship (5) and then subtracted from the data.

Estimation of source waveform and propagation characteristics directly from the data

In those cases in which scattered surface waves are present in the data, the incident field is mainly determined by the direct surface wave; direct body waves are present, but are generally small compared to the direct surface wave. Then, the direct surface wave can be clearly distinguished from the data and, consequently, can be used to directly estimate both the source waveform and the shallow propagation characteristics.

To that aim, we make two assumptions. The first is that we can neglect the depth dependence of $v_{33}^{G,s}$ if the heterogeneities are present in the shallow subsurface. (From tests on synthetic data, we have found that depth errors up to approximately one dominant wavelength of the Rayleigh wave have little effect on our method.) The second assumption is that the background medium is laterally invariant and, hence, $v_{33}^{G,s}(\mathbf{x}'|\mathbf{x}) = v_{33}^{G,s}(r)$, where R is the lateral distance between x' and x. This assumption limits the number of shots that can be taken into account simultaneously in the inversion (8) since many shots, that are located far apart, illuminate a large area that can generally not be considered as laterally invariant. We now parameterize $v_{33}^{G,s}$ [$= v_{33}^{G,s}(r)$] as follows:

$$v_{33}^{G,s}(\mathbf{x}'|\mathbf{x}) = F(r)\exp(i\omega r/c_R), \tag{9}$$

where c_R is the Rayleigh wave speed that is assumed to be constant within a small frequency band, but may differ for different frequency bands. In this way, dispersion is taken into account (if it is not too severe). Furthermore, the function F is a smooth amplitude function that accounts for the smooth dispersive part of $v_{33}^{G,s}$, while the exponential term accounts for the rapid changes in phase of $v_{33}^{G,s}$. This parameterization is motivated by the high-frequency asymptotic expressions for the surface-wave Green's function for a laterally invariant medium that are given in Aki and Richards (1980, section 7.4). According to equations (2) and (9), the direct Rayleigh wave is now parameterized as

$$v_3^{inc}(\mathbf{x}, \mathbf{x}^s) = W[F(r)\exp(i\omega r/c_R)], \tag{10}$$

where r is the distance between x and x^s. For each shot separately, we estimate the source and shallow propagation effects (i.e., W, F, and c_R) from this direct surface wave. To this aim, v_3^{inc} is first isolated by application of a cosine-squared time window. To take dispersion into account, we separate v_3^{inc} into frequency bands that have an approximately constant Rayleigh wave speed. We subsequently estimate c_R, W, and F for each frequency band separately. The Rayleigh wave speed c_R is estimated from the slope present in v_3^{inc}. We then estimate w in an ad hoc way by taking it equal to the direct wave for some chosen offset r_0 after removing the time delay caused by wave speed c_R, i.e., $W = \exp(-i\omega r_0/c_R)v_3^{inc}(r_0)$. For r_0, we choose an offset for which v_3^{inc} can be separated from other waves like head waves, higher-mode surface waves, and scattered surface waves. After estimating c_R and W, substitution in equation (10) yields an estimate for the amplitude F. It is noted that the estimated W not only represents the characteristics of the source, but also of the geophone and the recording system. Having obtained estimates for c_R and F, we have an estimate for $v_{33}^{G,s}$ and, consequently, for $G_3^{shallow}$

Although the parameterization for $v_{33}^{G,s}$ has a theoretical basis, the estimation of W (and subsequently F) is ad hoc, and the estimated W for a specific shot generally differs from the actual source signature of that shot. However, it can be deduced from the Born inversion method discussed in (Cohen et al., 1986) that, even if a source with erroneous frequency characteristics is used, a contrast function ξ can be obtained that "explains" the actual data. (Those authors apply their method to compressional waves, but the same argument holds for Rayleigh waves.) The contrast thus obtained may be different from the actual contrast. Since our objective is the removal of scattered surface waves rather than the determination of the actual contrast, errors in the source waveform play a minor role in the process of removing scattered surface waves.

RESULTS FOR TWO DIFFERENT FIELD DATA SETS

To evaluate our method, we have applied it to two field-data sets. The first data set was recorded during a "controlled" experiment where the near-surface scatterer distribution consisted of a (known) concrete dam. The second data set consists of a seismic line in a region with severe surface-wave scattering where the near-surface scatterer distribution was not known.

Grevelingen data: Objective and geometry

Early in 1993, we performed a field experiment on a tidal flat near a concrete dam (the "Grevelingendam") in the Province of Zeeland, in southwest Netherlands. Its objective was to investigate if a dispersive $G_3^{shallow}$ could be estimated directly from the data and to validate the imaging procedure for a known near-surface distribution of scatterers. This site showed negligible topographic variation except for the dam that was the only scattering object present and, hence, the shallow scatterer distribution was known.

The acquisition geometry is shown in Figure 1. The sources were located near the surface and consisted of 125 g of dynamite. We used three-component 10 Hz geophones at the surface, but in this paper, we consider only the vertical components. For each shot, eight geophones were placed in a straight line 100 m away from the foot of the dam. We chose a geophone spacing of 2 m; this small spacing avoided spatial aliasing of the surface waves in the common-shot domain. From experiments performed in this area by Snieder (1987) and Gabriels et al. (1987), the Rayleigh wave speed was approximately known, and we used this knowledge to choose the geophone spacing. For the shot spacing, we chose 8 m. We combined the sets of eight geophones for 30 shots in such a way that we obtained geophone offsets ranging from 2 m up to 480 m. Because of the lateral invariancy of the site, the variation between different shots was expected to be small.

Grevelingen data: Estimation of W and $G_3^{shallow}$

The shot record of the vertical component for the offsets 4-480 m is shown in Figure 2, Several strongly dispersive modes of the direct Rayleigh wave can be observed. The fundamental mode is the slowest one, and it is well separated from the higher modes for offsets larger than approximately 80 m. Especially at the small offsets, we can see the Rayleigh waves reflected from the dam: around t = 2.4 s, the reflected fundamental mode is visible, while the reflected higher modes are present at earlier times. We can also observe some high-velocity body-wave reflections from the deeper part of the subsurface (these are visible at early times).

To estimate W and $G_3^{shallow}$ from these data, first a cosine-squared time window is applied for isolating the fundamental direct Rayleigh wave. It is noted that, for offsets up to about 80 m, the fundamental mode interfers with the higher modes. By considering the amplitude spectrum, we found that the main energy is in the frequency range of 5-12 Hz; this spectrum is shown in Figure 3 for an offset of 200 m.

By examining the direct wave within the frequency bands 5-9 Hz and 8-12 Hz, respectively, we have found that the phase velocity c_R of the Rayleigh wave can be considered constant within each of these bands. The frequency band between 5-9 Hz of the fundamental mode is shown in Figure 4. From the slope present in this figure, we estimate the phase velocity at 173 m/s. For the interval 8-12 Hz, we have found an estimate of 146 m/s for the phase velocity.

Since we used 10 Hz geophones, the amplitude and phase of the recorded data are affected for frequencies around and below 10 Hz. Despite the fact that these distortions can affect the image of the dam, the modeled reflections from the dam are still expected to be accurate because of the data-fitting nature of our method.

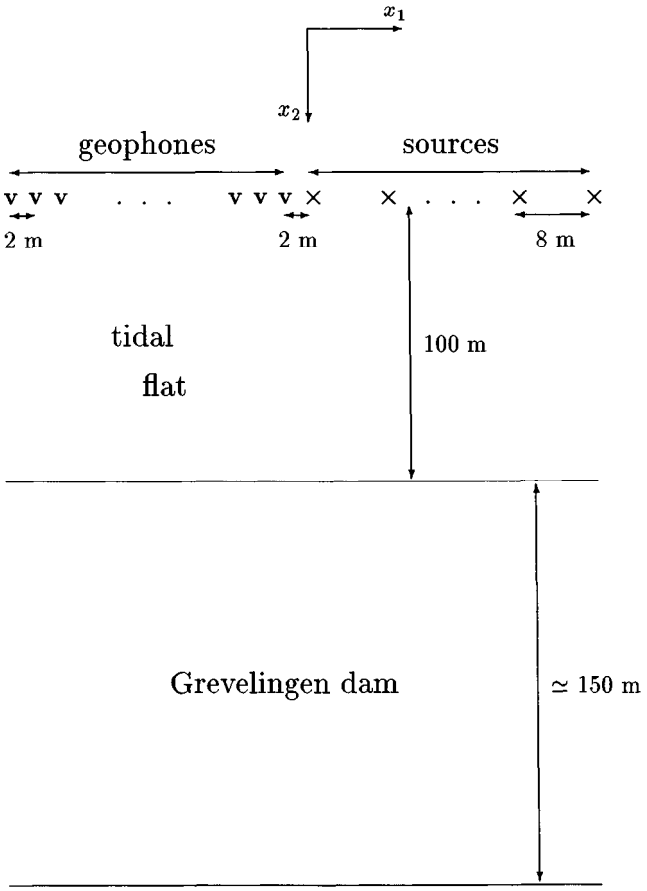

FIG. 1. Layout of the Grevelingen field experiment.

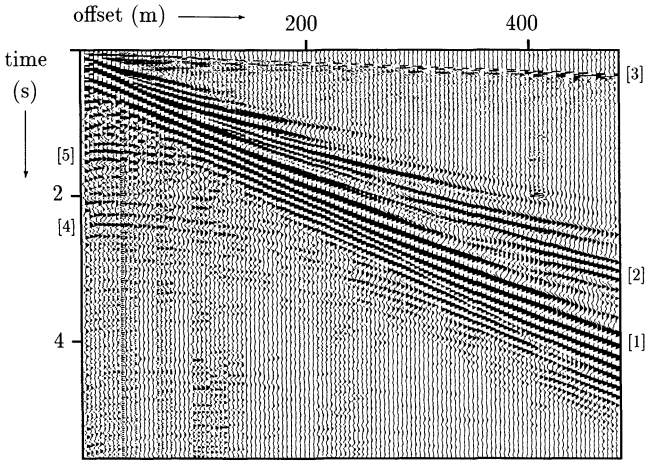

FIG. 2. Vertical velocity component of the Grevelingen data. The numbers between square brackets indicate the different wave types: (1) direct fundamental mode of the Rayleigh wave, (2) direct higher modes of the Rayleigh wave, (3) body-wave reflections from the deeper subsurface layers, (4) fundamental mode reflected by the dam, and (5) higher-mode reflections.

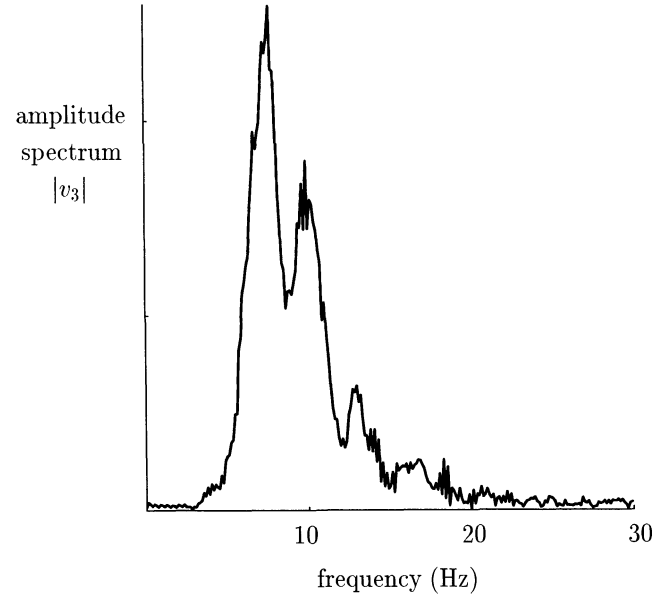

FIG. 3. Amplitude spectrum of the Grevelingen data for an offset of 200 m. In our test, we consider only the frequency range 5-12 Hz, which contains the main energy.

For the two separate frequency bands, we choose the source waveform w equal to the waveform of the fundamental mode at offset r_0 = 200 m (for this offset, v_3^{inc} is reasonably well separated from the higher-mode Rayleigh waves and the reflections from the dam). We then estimate $v_{33}^{G,s}(r)$ using c_R, W, and equations (9)-(10). Finally, we obtain $G_3^{shallow}$ from equation (6).

Grevelingen data: Results

For the frequency bands 5-9 Hz and 8-12 Hz, we have separately estimated the near-surface distributions ξ by minimizing equation (8) iteratively. The two distributions consist of 5151 cells: 101 cells in the inline direction and 51 in the crossline direction (the cell size is 4 m x 4 m). The geometry for these distributions is shown in Figure 5. Since the parameterization (10) is suitable only for offsets larger than 80 m, we estimate the near-surface distribution at distances larger than 80 m from the shot line. For smaller offsets, several modes of the direct wave are interfering, which makes it difficult to estimate the propagation characteristics of the incident wave and the Green's function.

For the frequency band 5-9 Hz, the estimated horizontal distribution ξ, obtained after 10 iterations, is shown in Figure 6. In this illustration, a coherent image of the dam is visible at a distance of approximately 160 m from the shot line. Apparently, the main scattering from the dam occurs at the foundation below the middle of the dam. Within the 8-12 Hz band, a much less coherent image of the dam was obtained. We assume that this is because of the fact that, within this band, the fundamental mode being imaged contains significantly less energy than the higher modes.

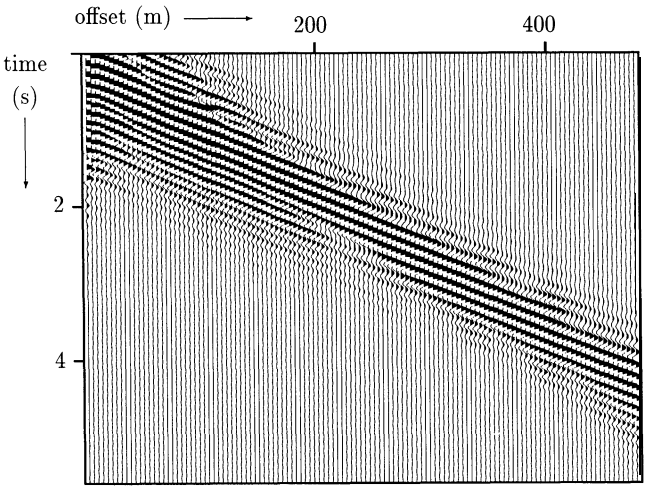

FIG. 4. Isolated fundamental model of the direct Rayleigh wave for the frequency band 5-9 Hz (Grevelingen data).

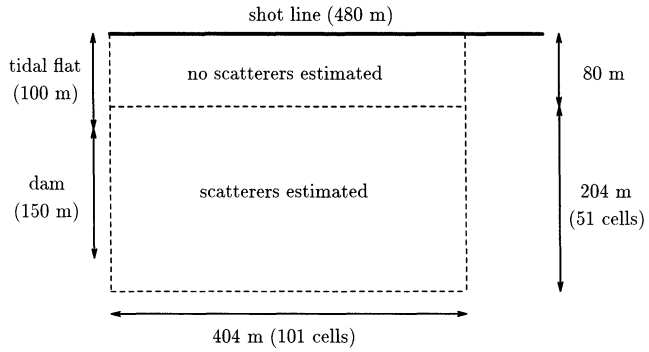

FIG. 5. Top view of the geometry for the scatterer distributions estimated in the test with the Grevelingen data.

Having obtained estimates of the scatterer distributions, we now calculate the reflections of the fundamental mode that have been reflected at the dam. Subtraction of these reflections from the recorded response (shown in Figure 2) results in the data that are shown in Figure 7. Despite the fact that we removed the scattered surface waves only within the 5-12 Hz band, the response in Figure 7 contains all frequencies present in the measurements. We observe that the reflections of the fundamental mode have been attenuated significantly.

Amoco data: Objective and geometry

The second test on field data concerns a seismic line recorded by Amoco in 1991. In certain parts of that line, high-amplitude scattered surface waves were present that were not suppressed sufficiently by stacking. The objective of this second test was to attenuate the scattered surface waves as much as possible and to leave the body-wave reflections intact.

The line was recorded with dynamite sources and vertical geophones located at the surface. The source and receiver

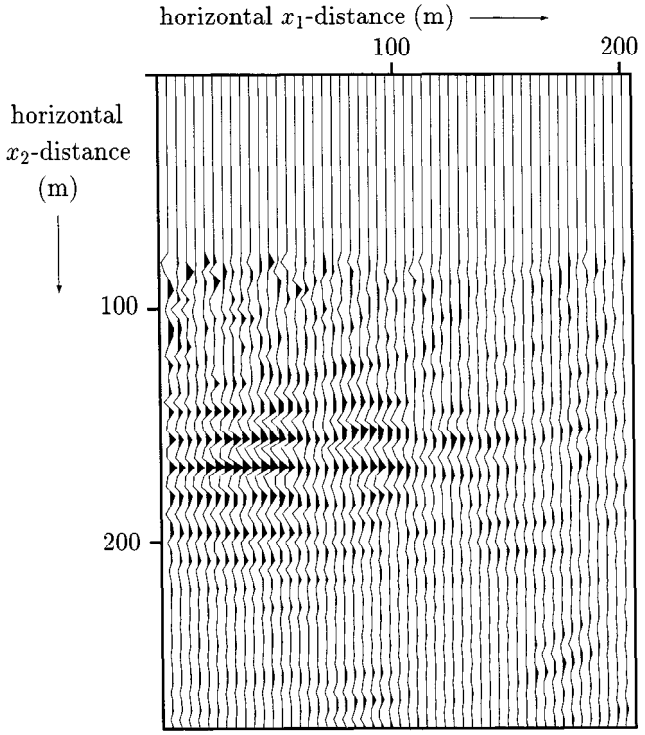

FIG. 6. Image of the dam for the frequency band 5-9 Hz. The horizontal x_1-distance is parallel to the dam and the horizontal x_2-direction is perpendicular to it.

spacings were 25 m, and the number of receivers per shot was 100. For each shot, the minimum and maximum offsets were 25 m and 2500 m, respectively.

The vertical velocity recording for a typical shot is shown in Figure 8. The dominant linear event is the direct Rayleigh wave that is somewhat dispersive, and the strong hyperbolic events correspond to scattered Rayleigh waves. From the shape of the hyperbolas, we conclude that most of the scattered waves arrive from the crossline direction. We can distinguish some body-wave reflections between t = 0.75 s and t = 1.3 s. The head waves can also be observed. Since they contain less energy than the direct Rayleigh wave, the scattered head waves (if present) are small compared to the scattered Rayleigh waves. The data show no evidence of the presence of scattered head waves.

Amoco data: Estimation of $\boldsymbol{W}$ and $\boldsymbol{G_3^{shallow}}$

As a first step, we isolate the direct Rayleigh wave by application of a (cosine-squared) time window (in this data set, no significant higher modes are present). Its energy is present mainly in the 7-37-Hz frequency range. By examining the direct wave within the frequency bands 7-23.5 Hz and 20.5-37 Hz, respectively, we have found that the phase velocity c_R of the Rayleigh wave is approximately constant within each of these bands. For the frequency range 7-23.5 Hz, we have estimated the phase velocity at 1825 m/s; for the interval 20.5-37 Hz we have found an estimate of 1795 m/s for the phase velocity.

Unlike the Grevelingen data, the different sources are not assumed to be identical and, therefore, we estimate a different source signature for each different shot. For this estimation, we follow the procedure described above, where we choose the offset r. = 1250 m. Finally, for each separate shot and frequency band, we use c_R and W together with equation (9) to estimate $v_{33}^{G,s}$ (Y), which is subsequently used with equation (6) to obtain $G_3^{shallow}$.

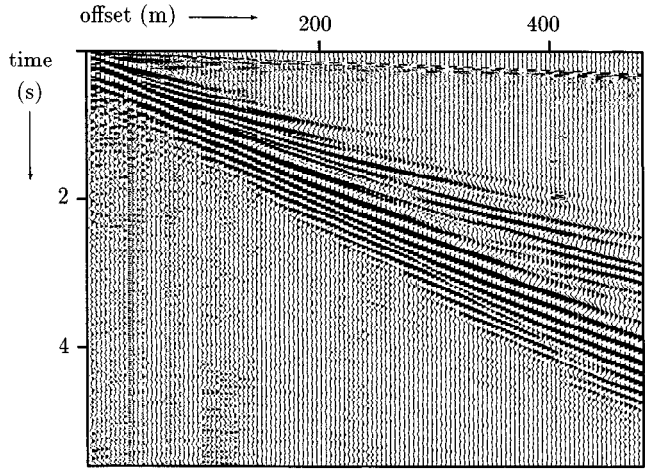

FIG. 7 Shot record of the vertical velocity component of the Grevelingen data after removing the reflected fundamental mode of the Rayleigh wave (within the 5-12 Hz band).

Amoco data: Results

For each separate frequency band and shot, we estimate a distribution ξ by solving requirement (8) iteratively. These distributions consist of 9490 cells: 130 cells in the inline direction and 73 cells in the crossline direction. The cell size is 25 m x 25 m. For the present test, this cell size appears to be small enough, although tests with synthetic data have shown that a smaller cell size is generally preferable (Blonk and Herman, 1994).

For the shot shown in Figure 8, the estimated distributions, after performing 15 iterations, are shown in Figures 9a and 9b for the lower and higher frequency ranges, respectively. Because of the time window h^{time} [see equation (7)], we cannot estimate the distribution close to the seismic line, as can be seen in Figure 9a. Since $v_{33}^{G,s}(\boldsymbol{r})$ is available only for offsets $\boldsymbol{r} \leq 2500$ m, we do not estimate scatterers at distances larger than 2500 m from the source.

Having obtained the distributions shown in Figures 9a and 9b, we compute the scattered surface waves for the shot record of Figure 8. These scattered waves are subsequently subtracted from the recorded data; the result is shown in Figure 10. We observe that the scattered surface waves are attenuated (we also subtracted the modeled direct surface wave). In principle, linear remnants of Rayleigh waves can now be removed by additional prestack wavenumber-frequency filtering.

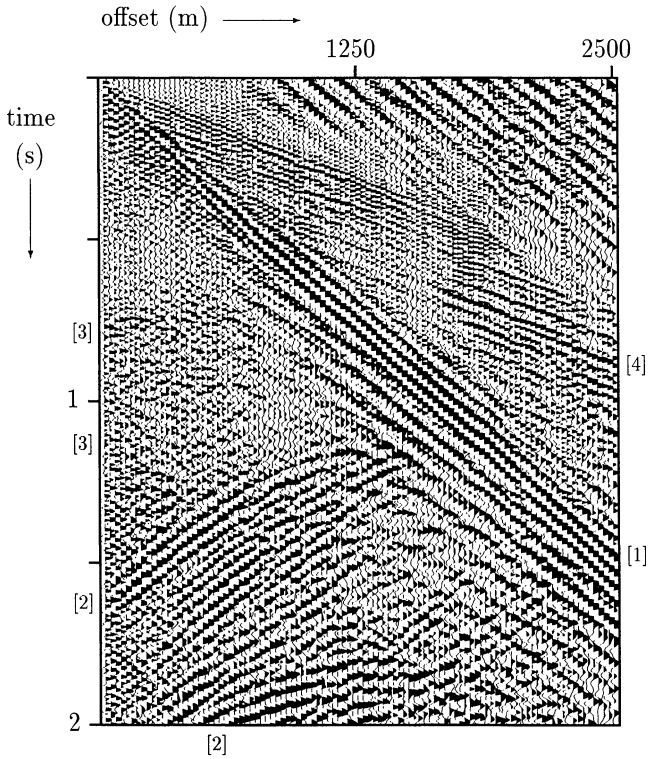

FIG. 8. A typical shot record (vertical velocity) from a line recorded by Amoco (the number of traces is 100, the receiver spacing is 25 m, and the time sampling interval is 4 ms). The direct surface'wave is indicated by (1), crossline-scattered surface waves (hyperbolic events) by (2) body-wave reflections from the deeper subsurface by (3) and head waves by (4).

To assess if our method does not attenuate reflections, we applied our technique to 30 adjacent shots. In Figure lla, the 30-fold stack is shown (without application of our method). For comparison, the same stack, obtained after the application of our method, is shown in Figure llb. Apart from the surface-wave removal, all processing and display parameters are the same for Figures lla and llb. We can now make two observations. The first one is that reflections present in the original stack are still present in the stack after attenuation of the scattered surface waves. The second one is that the continuity of the reflections of Figure llb appears to be better than in Figure lla. Also, Figure lla shows linear remnants of crossline scattered Rayleigh waves that are more pronounced than the ones shown in Figure llb. Apparently, scattered surface waves have been attenuated without much affect on the deeper reflections. This is particularly visible in the lower part of the stack.

The effect of our method on the stack can also be quantified by considering the difference between the stacks shown in Figures lla and llb, as shown in Figure 12. We observe that the difference consists mainly of linear noise patterns having positive dips (from upper left to lower right), as well as negative dips (from lower left to upper right). A part of the linear patterns having a positive dip corresponds with the direct surface wave. From the presence of some horizontal events, we conclude that our method has also affected reflections to a certain extent, in particular between 0.8 s and 1.0 s.

We realize that the application of poststack wavenumber-frequency filtering could probably also improve the stack considered in our test because the scattered surface waves can be identified quite clearly (strongly dipping, unaliased patterns as opposed to horizontal reflectors). However, poststack filtering methods are based on assumptions regarding the geology and may therefore deteriorate the lateral resolution of the stack.

DISCUSSION AND CONCLUSIONS

In a previous paper, we discussed an elastodynamic inverse scattering method for eliminating scattered surface waves. By applying the method to synthetic data, we concluded that this method was effective and robust; its main sensitivity concerned the Rayleigh wave speed. This type of sensitivity was comparable to the sensitivity to body wave

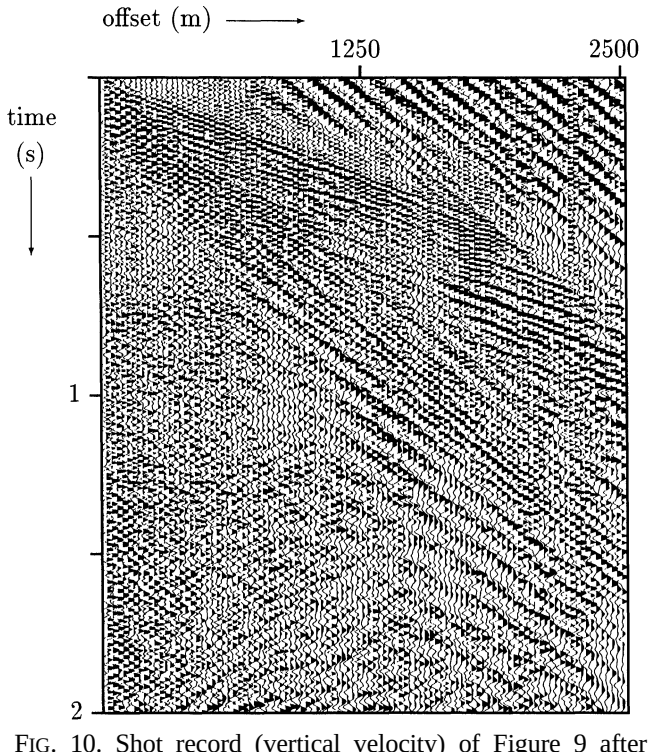

FIG. 10. Shot record (vertical velocity) of Figure 9 after attenuation of the scattered surface waves.

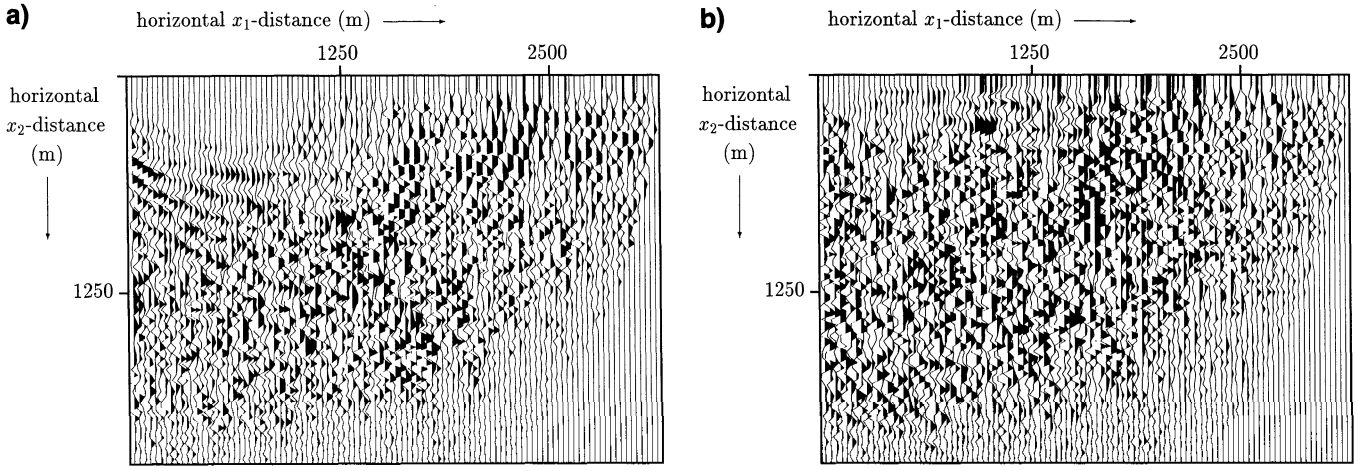

FIG. 9. Estimated near-surface distributions for the shot record shown in Figure 8 for the frequency ranges (a) 7-23.5 Hz and (b) 20.5-37 Hz. The horizontal x_1 -distance is parallel to the source-receiver line and the horizontal x_2-direction is perpendicular to it

speed of methods like linearized inversion and prestack depth migration.

In the present paper, we have extended this method with a procedure for estimating the Rayleigh wave speed and other propagation characteristics directly from the data (taking dispersion into account). Furthermore, we have applied the method to two different data sets: the first data set was recorded in a "controlled" experiment, where the shallow scatterer distribution (the Grevelingen Dam) was known, while the second data set was a seismic line strongly contaminated by scattered surface waves. From the first data set, we conclude that we can estimate the source and propagation characteristics with sufficient accuracy directly from the data. Also, we have obtained a correct image of the dam. The test with the second data set has shown that our method effectively attenuates scattered surface waves without attenuating deep body-wave reflections too much.

In general, we expect a further reduction of the near-surface noise when many shots are taken into account simultaneously in the estimation of the shallow distribution ξ. Different shots from a swath survey would be preferable because the subsurface is then illuminated from different directions. However, for a multishot inversion, at least a more sophisticated estimate for W is required for each shot.

In many cases, the background medium is laterally varying. In that case, ray-tracing techniques would have to be used for computing $v_{33}^{G,s}$ and the computation of $G_3^{shallow}$ would be based on an estimate of a shallow velocity model. This requires the development of a ray-trace tomography method for surface waves.

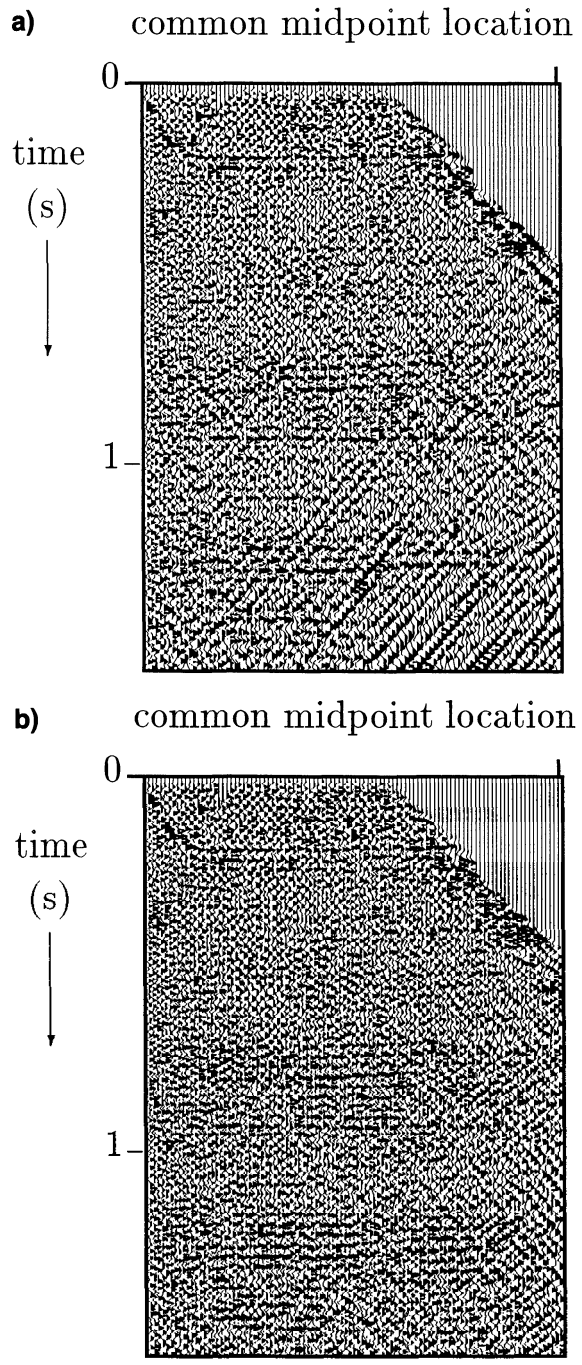

FIG. 11. Stack (30-fold) of (a) Amoco data and (b) stack after attenuation of scattered surface waves. All other processing and display parameters are identical.

ACKNOWLEDGMENTS

The research presented in this paper was sponsored by the Dutch Technology Foundation (STW) and by Shell Research. This support is gratefully acknowledged. We would like to thank Amoco for providing us with field data and also

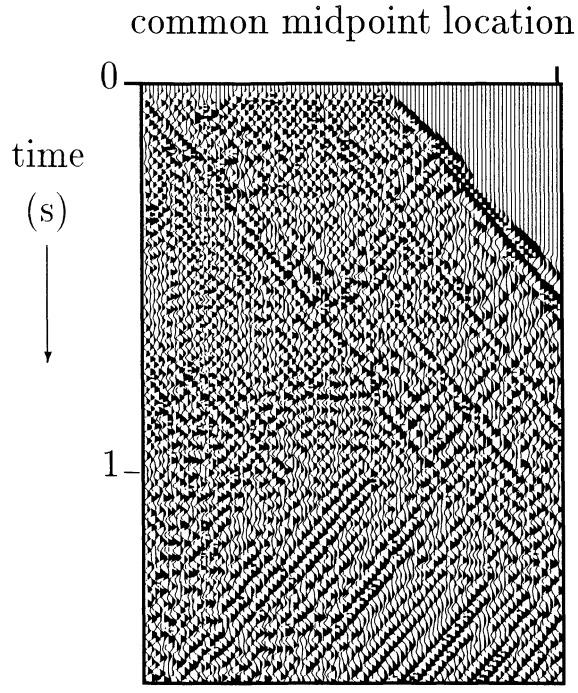

FIG. 12. Difference of the stacks shown in Figures lla and llb. Its main part consists of linear patterns (both positive and negative dip). The horizontal reflectors that are present indicate that our method has also imaged some of the reflections from the deeper layers. (All processing and display parameters are identical to those of Figure 11.)

Klaas-Jan Koster from Amoco and Eric Verschuur from Delft University for their help and advise. The field crew of the Department of Mining and Petroleum Engineering, as well as the students from the Departments of Applied Physics, Applied Mathematics and Mining and Petroleum Engineering (Delft University), are acknowledged for their help in performing the field experiment at the Grevelingen Dam. The constructive comments of the reviewers are also gratefully acknowledged.

REFERENCES

Aki, K., 1969, Analysis of the seismic coda of local ea.rthqu akes as scattered waves: J. Geophys. Res., 74, 615-631.

Aki, K., and Richards, P. G., 1980, Quantitative seismology, theory and methods: W. H. Freeman and Co.

Blonk, B., and Herman, G. C., 1993, An iterative inverse scattering method for the removal of scattered surface waves: 63th Ann. Internat. Mtg., Soc. Expl. Geophys., Expanded Abstracts, 606-609.

——— 1994, Inverse scattering of surface waves: A new look at surface consistency: Geophysics, 59, 963-972.

Cohen, J. K., Hagin, F. G., and Bleistein, N., 1986, Three-dimensional Born inversion with an arbitrary reference: Geophysics, 51, 1552-1558.

Gabriels, P., Snieder, R., and Nolet, G., 1987, In-situ measurements of shear-wave velocity in sediments with higher-mode Rayleigh waves: Geophys. Prosp., 35, 187-196.

Kleinman, R. E., and van den Berg, P. M., 1991, Iterative methods for solving integral equations: Radio Science, 26, 175-181.

Snieder, R., 1987, Surface wave scattering theory: Ph.D. thesis, University of Utrecht .

Yilmaz, O., 1988, Seismic data processing: Soc. of Explor. Geophys.